JCI insight

RESEARCH ARTICLE

The atypical antipsychotic quetiapine induces hyperlipidemia by activating intestinal PXR signaling

Zhaojie Meng,[1] Taesik Gwag,[1] Yipeng Sui,[1] Se-Hyung Park,[1] Xiangping Zhou,[2] and Changcheng Zhou[1]

[1]Department of Pharmacology and Nutritional Sciences, University of Kentucky, Lexington, Kentucky, USA. [2]Department of Neurology, SUNY Upstate Medical College, Syracuse, New York, USA.

Quetiapine, one of the most prescribed atypical antipsychotics, has been associated with hyperlipidemia and an increased risk for cardiovascular disease in patients, but the underlying mechanisms remain unknown. Here, we identified quetiapine as a potent and selective agonist for pregnane X receptor (PXR), a key nuclear receptor that regulates xenobiotic metabolism in the liver and intestine. Recent studies have indicated that PXR also plays an important role in lipid homeostasis. We generated potentially novel tissue-specific PXR-KO mice and demonstrated that quetiapine induced hyperlipidemia by activating intestinal PXR signaling. Quetiapine-mediated PXR activation stimulated the intestinal expression of cholesterol transporter Niemann-Pick C1-Like 1 (NPC1L1) and microsomal triglyceride transfer protein (MTP), leading to increased intestinal lipid absorption. While NPC1L1 is a known PXR target gene, we identified a DR-1–type PXR-response element in the MTP promoter and established MTP as a potentially novel transcriptional target of PXR. Quetiapine's effects on PXR-mediated gene expression and cholesterol uptake were also confirmed in cultured murine enteroids and human intestinal cells. Our findings suggest a potential role of PXR in mediating adverse effects of quetiapine in humans and provide mechanistic insights for certain atypical antipsychotic-associated dyslipidemia.

Introduction

Quetiapine is one of the most prescribed second-generation (atypical) antipsychotics and is commonly used for the treatment of several psychiatric conditions including bipolar disorders, schizophrenia, major depressive disorder, and general anxiety disorder (1–3). Quetiapine is the only approved atypical antipsychotic in the US for use as monotherapy to treat bipolar disorders that affect more than 1% of the global population and often require life-long medication (1, 4, 5). Quetiapine has documented efficacy and a reduced risk for extrapyramidal symptom as compared with several other antipsychotics (2, 4, 6–8). However, the use of quetiapine has been associated with dyslipidemia and an increased risk of cardiovascular disease (CVD) in patients (8–13). Findings from CATIE schizophrenia trial demonstrated that quetiapine was associated with an increased 10-year CVD risk (9). Another clinical study found that switching from quetiapine to aripiprazole, a newer atypical antipsychotic, was associated with large reductions in predicted 10-year CVD risk (10). The quetiapine-associated CVD risk can be explained, at least in part, by its dyslipidemic effects. A large-scale clinical study including more than 85,000 subjects concluded that treatment with quetiapine significantly increased the risk of developing hyperlipidemia (11). Several other studies also confirmed that the use of quetiapine was associated with increased serum lipid levels including elevated total and low-density lipoprotein (LDL) cholesterol levels (8, 12, 13). However, the underlying mechanisms responsible for quetiapine's dyslipidemic effects remain unknown, which poses a serious health challenge for patients undergoing long-term treatment with quetiapine.

We and others have previously identified several clinically used drugs with dyslipidemic effects, including ritonavir, amprenavir, rifampicin, and cyclosporine A, as potent agonists of pregnane X receptor (PXR; also known as steroid and xenobiotic receptor [SXR]) (14–18). PXR is a nuclear receptor activated by numerous endogenous hormones, dietary steroids, pharmaceutical drugs, and environmental chemicals (14, 17, 19). PXR functions as a xenobiotic sensor that induces expression of genes required for xenobiotic metabolism in liver and intestine, such as cytochrome P450s (CYP) (17, 19). In the past 2 decades, the

Authorship note: ZM and TG contributed equally to this work.

Conflict of interest: The authors have declared that no conflict of interest exists.

Submitted: October 19, 2018
Accepted: January 3, 2019
Published: February 7, 2019

Reference information:
JCI Insight. 2019;4(3):e125657.
https://doi.org/10.1172/jci.insight.125657.

function of PXR in drug and xenobiotic metabolism has been extensively studied, and the role of PXR as a xenobiotic sensor has been well established (19, 20). Recent studies have revealed potentially novel functions of PXR in the regulation of lipid homeostasis (16, 18, 21–25). While PXR has been shown to regulate multiple hepatic and intestinal genes involved in lipid homeostasis in different animal models (18, 19, 22, 23, 25), the tissue-specific role of PXR in lipid homeostasis remains elusive.

In this study, we investigated the potential contribution of PXR signaling toward quetiapine's dyslipidemic effects in mice. We found that quetiapine, but not the relatively new atypical antipsychotic aripiprazole, is a potent PXR-selective agonist. We also generated tissue-specific PXR-KO mice and demonstrated that quetiapine elicits hyperlipidemia by targeting intestinal PXR signaling in mice.

Results

The atypical antipsychotic quetiapine is a PXR-selective agonist. We examined 2 commonly prescribed atypical antipsychotics, quetiapine and aripiprazole, for PXR activation by transfection assays. Since PXR exhibits considerable differences in its pharmacology across species (17, 19, 26), we tested whether quetiapine and aripiprazole affect human (h) and mouse (m) PXR activity. The potent species-specific PXR ligands rifampicin and pregnenolone 16α-carbonitrile were used as the positive controls for hPXR and mPXR, respectively. Interestingly, quetiapine — but not aripiprazole — activated both hPXR and mPXR (Figure 1, A and B). Dose-response analysis demonstrated that the half-maximal effective concentrations (EC_{50}) of quetiapine were 13.4 μM for hPXR and 10.6 μM for mPXR (Figure 1, C and D).

To determine whether quetiapine activates specifically on PXR, we also evaluated the ability of quetiapine to activate a panel of other nuclear receptors, including retinoid acid receptor–α (RARα), retinoid X receptor (RXR), farnesoid X receptor (FXR), liver X receptor–α (LXRα), peroxisome proliferator-activated receptor–α (PPARα), PPARγ, vitamin D receptor (VDR), constitutive androstane receptor (CAR), estrogen receptor–α (ERα), and ERβ. Quetiapine can activate all 3 forms of PXR — including hPXR, mPXR, and rat PXR (rPXR) — but was unable to activate any other nuclear receptors (Figure 1E). These data suggest that quetiapine is a PXR-specific agonist.

Quetiapine binds to PXR and modulates PXR and coregulator interactions. Most natural and synthetic nuclear receptor agonists act as ligands by directly binding to the nuclear receptor ligand binding domain. Thus, we next sought to determine whether quetiapine can directly bind to purified PXR proteins in vitro using a time-resolved fluorescence resonance energy transfer (TR-FRET) PXR competitive binding assay. Consistently, quetiapine — but not aripiprazole — can displace fluorescently labeled tracer from the PXR ligand-binding domain (LBD) in a dose-dependent manner (Figure 2A). The IC_{50} for quetiapine binding to PXR was determined to be 12.1 μM, a value in the range of other known PXR ligands (19, 27).

In the absence of ligands, many nuclear receptors form a complex with corepressors that inhibit transcriptional activity of the complex (28). When a ligand binds to its nuclear receptor, a conformational change occurs, resulting in dissociation of corepressor and recruitment of coactivator proteins (28). Nuclear receptor coregulators, therefore, are essential for nuclear receptor activation. We then used a mammalian 2-hybrid assay to evaluate the impact of quetiapine on PXR coregulator interactions (16, 26). Similar to the known hPXR ligand rifampicin, quetiapine promoted the specific interactions between PXR and the coactivators steroid receptor coactivator–1 (SRC-1) and PPAR binding protein (PBP) (Figure 2B), but it disrupted the interactions between PXR and corepressors, including nuclear receptor corepressor (NCoR) and silencing mediator of retinoid and thyroid hormone (SMRT) (Figure 2C). Thus, binding of quetiapine to PXR inhibits PXR/corepressor interaction and promotes PXR/coactivator recruitment, thereby inducing PXR transcriptional activation.

Generation of intestine-specific PXR-KO mice. We and others previously demonstrated that modulation of PXR activity can affect lipid metabolism and plasma lipid levels in several different mouse models (16, 18, 21, 22, 24, 25). However, the detailed mechanisms through which PXR signaling regulates lipid homeostasis remain elusive. PXR is expressed at high levels in both liver and intestine, which are essential for whole-body lipid homeostasis. To define the tissue-specific role of PXR in xenobiotic and lipid metabolism, we have recently successfully generated hepatocyte-specific PXR-deficient mice (termed as $PXR^{\Delta Hep}$) by crossing mice carrying PXR flox alleles ($PXR^{fl/fl}$) with Albumin-Cre transgenic mice (29). For the current study, $PXR^{fl/fl}$ mice were also crossed with Villin-Cre transgenic mice to generate intestinal epithelial cell-specific (IEC-specific) PXR-deficient mice ($PXR^{\Delta IEC}$) (Supplemental Figure 1A; supplemental material available online with this article; https://doi.org/10.1172/jci.insight.125657DS1). PCR analysis of genomic DNA indicated that the Cre-mediated recombination was specific to the intestine of $PXR^{\Delta IEC}$ mice (Supplemental Figure 1B).

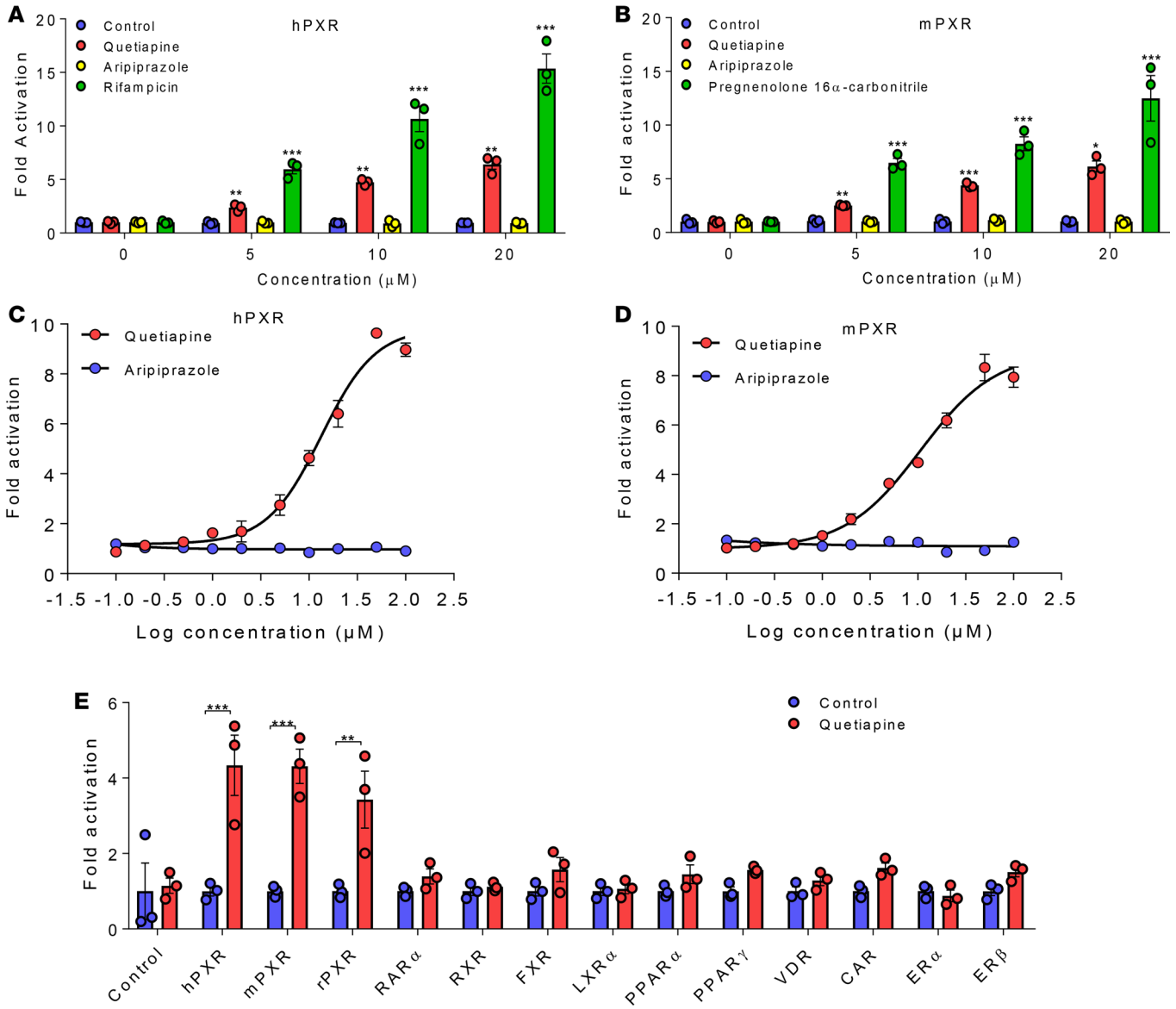

Figure 1. The atypical antipsychotic quetiapine is a PXR-selective agonist. (**A** and **B**) HepG2 cells were transfected with (**A**) full-length hPXR together with hPXR reporter (CYP3A4-luc) or (**B**) full-length mPXR together with mPXR reporter ($[CYP3A2]_3$-luc) and CMX–β-galactosidase control plasmids. Cells were then treated with DMSO control, quetiapine, aripiprazole, and rifampicin (hPXR ligand) or pregnenolone 16α-carbonitrile (mPXR ligand) at the indicated concentrations for 24 hours (n = 3, 1-way ANOVA, $^*P < 0.05$, $^{**}P < 0.01$, and $^{***}P < 0.001$ compared with control group). (**C** and **D**) HepG2 cells were transfected with hPXR and CYP3A4-luc reporter (**C**) or mPXR and $(CYP3A2)_3$-luc reporter (**D**) together with CMX–β-galactosidase plasmids. Cells were then treated with quetiapine or aripiprazole at the indicated concentrations for 24 hours (n = 3). (**E**) HepG2 cells were transfected with a GAL4 reporter and a series of GAL4 plasmids in which the GAL4 DNA-binding domain is linked to the indicated nuclear receptor ligand–binding domain. Cells were treated with DMSO control or 20 μM quetiapine for 24 hours (n = 3, Student's t test, $^{**}P < 0.01$, $^{***}P < 0.001$ compared with control group).

As expected, the mRNA and protein levels of PXR were significantly decreased in the intestine but not in other major tissues, including liver of $PXR^{\Delta IEC}$ mice, as compared with $PXR^{fl/fl}$ mice (Figure 3, A and B), demonstrating the specific and efficient PXR deletion in the intestine of $PXR^{\Delta IEC}$ mice.

Quetiapine elicits hypercholesterolemia by targeting intestinal PXR signaling in mice. To evaluate the impact of quetiapine on PXR activity and lipid homeostasis in vivo, $PXR^{\Delta IEC}$, $PXR^{\Delta Hep}$, and their corresponding $PXR^{fl/fl}$ littermates were treated with 10 mg/kg body weight (BW)/day of quetiapine or vehicle control by oral gavage for 1 week. Quetiapine has been previously used to treat mice at the dose of 10 mg/kg/day for short-term exposure or 5 mg/kg/day for long-term exposure (30–32). Patients can be given a daily dose of quetiapine 300–800 mg for long-term treatment of bipolar disorders (1, 2). The 10 mg/kg/day quetiapine dose for mouse treatment is within or below the human dose range, when considering the interspecies

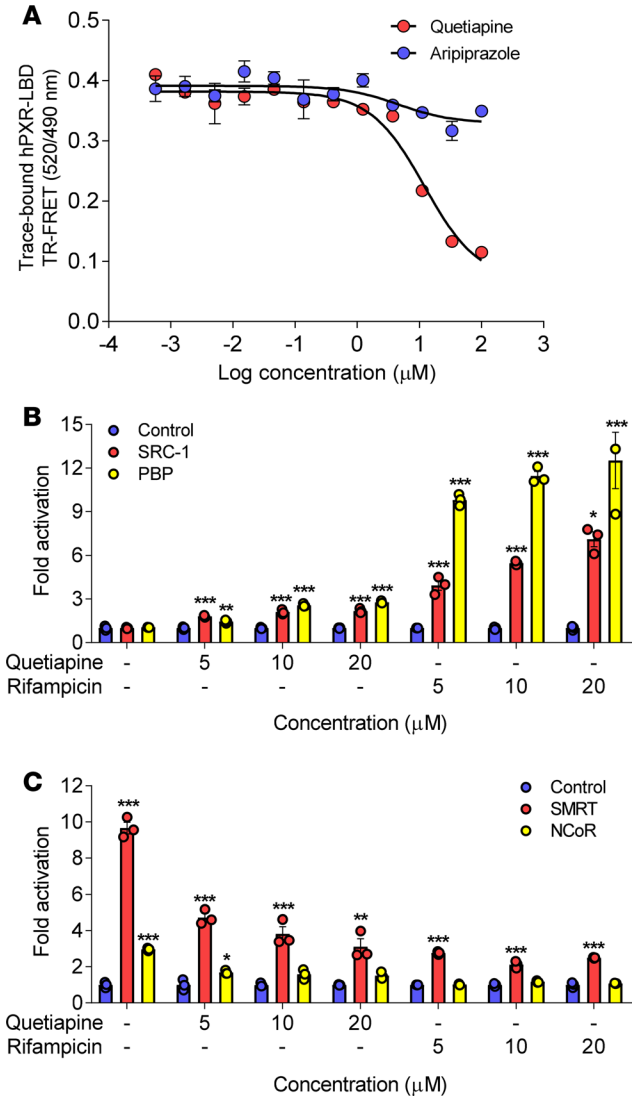

Figure 2. Quetiapine binds to PXR and modulates PXR and coregulator interactions. (**A**) Inhibition of FRET between fluorescein-labeled PXR ligand and recombinant GST-PXR by quetiapine or aripiprazole. Results are expressed as the signal from the fluorescein emission divided by the terbium signal to provide a TR-FRET emission ratio (n = 3). (**B** and **C**) HepG2 cells were transfected with a GAL4 reporter, VP16-hPXR vector, and expression vector for GAL4 DNA-binding domain or GAL4 DNA-binding domain linked to the receptor interaction domains of PXR coactivators (GAL4-SRC1 or GAL4-PBP) (**B**) or PXR corepressors (GAL4-SMRT or GAL4-NCoR) (**C**). Cells were treated with DMSO control, quetiapine, or rifampicin at the indicated concentrations for 24 hours. Data are shown as fold induction of normalized luciferase activity compared with DMSO control treatment (n = 3, 1-way ANOVA, $^{*}P < 0.05$, $^{**}P < 0.01$, and $^{***}P < 0.001$ compared with control group).

scaling factor between mice and human (12.3:1) (33, 34). Interestingly, treatment with quetiapine for only 1 week significantly increased plasma total cholesterol and atherogenic very-low-density lipoprotein (VLDL) and LDL cholesterol levels without affecting BW and fasting triglyceride levels in $PXR^{fl/fl}$ mice (Figure 3, C–F). Deficiency of intestinal PXR abolished the impact of quetiapine on plasma total and lipoprotein cholesterol levels.

We also performed similar quetiapine treatment in $PXR^{fl/fl}$ and $PXR^{\Delta Hep}$ littermates. As expected, $PXR^{\Delta Hep}$ mice used for this study had significantly reduced PXR expression in liver but not in intestine (Figure 4A). Quetiapine treatment did not affect BW in those mice, either (Figure 4B). Interestingly, quetiapine treatment had similar effects on plasma lipid levels in $PXR^{\Delta Hep}$ mice as it had in $PXR^{fl/fl}$ mice (Figure 4, C–E). Quetiapine can increase total, VLDL, and LDL cholesterol levels in both $PXR^{fl/fl}$ and $PXR^{\Delta Hep}$ mice. These results demonstrate that intestinal but not hepatic PXR signaling mediated hypercholesterolemia induced by quetiapine in mice.

Quetiapine-mediated PXR activation stimulates key intestinal lipogenic gene expression. Small intestine lipid absorption is the key step for lipid accumulation in the body (35), and we previously reported that PXR can regulate several key genes involved in intestinal lipid homeostasis including the essential cholesterol transporter Niemann-Pick C1-Like 1 (NPC1L1) (25). Gene expression analysis then confirmed that quetiapine treatment significantly increased the expression of bona fide PXR target genes such as CYP3A11 and MDR1a, as well as NPC1L1, in the intestine of $PXR^{fl/fl}$ but not $PXR^{\Delta IEC}$ mice (Figure 5, A and B). Interestingly, quetiapine-mediated PXR activation significantly stimulated the expression of another key gene required for intestinal lipid absorption and lipoprotein assembly, microsomal triglyceride transfer protein (MTP) (36), in $PXR^{fl/fl}$ mice, and deficiency of intestinal PXR abolished this induction (Figure 5B). Consistent with our previous studies (25), activation of PXR by quetiapine did not affect the intestinal expression of cholesterol efflux transporters ABCG5 and ABCG8 (Figure 5B). Immunoblotting and immunofluorescence staining also confirmed that quetiapine induced intestinal NPC1L1 and MTP protein levels in $PXR^{fl/fl}$ but not $PXR^{\Delta IEC}$ mice (Figure 5, C–E). Further, deficiency of hepatic PXR did not alter the impact of quetiapine on intestinal gene expression, as the expressional levels of NPC1L1, MTP, and other PXR target genes were also upregulated by quetiapine in the intestine of $PXR^{\Delta Hep}$ mice (Supplemental Figure 2).

MTP is a potentially novel transcriptional target of PXR. The role of PXR in transcriptionally regulating NPC1L1 expression has been previously demonstrated (25). However, the impact of PXR activation on MTP expression has not been reported. We next analyzed the promoters of MTP genes from different species and identified a conserved DR-1 type (direct repeat spaced by 1 nucleotide) of nuclear receptor responsive element (Figure 6A). This DR-1 element, which is different from a previously described NR2F1 potential binding site (37), is quite conserved across different species, including human, mouse, rat, dog, and chicken (Figure 6A). EMSA then confirmed that the PXR and RXR heterodimer was able to bind to

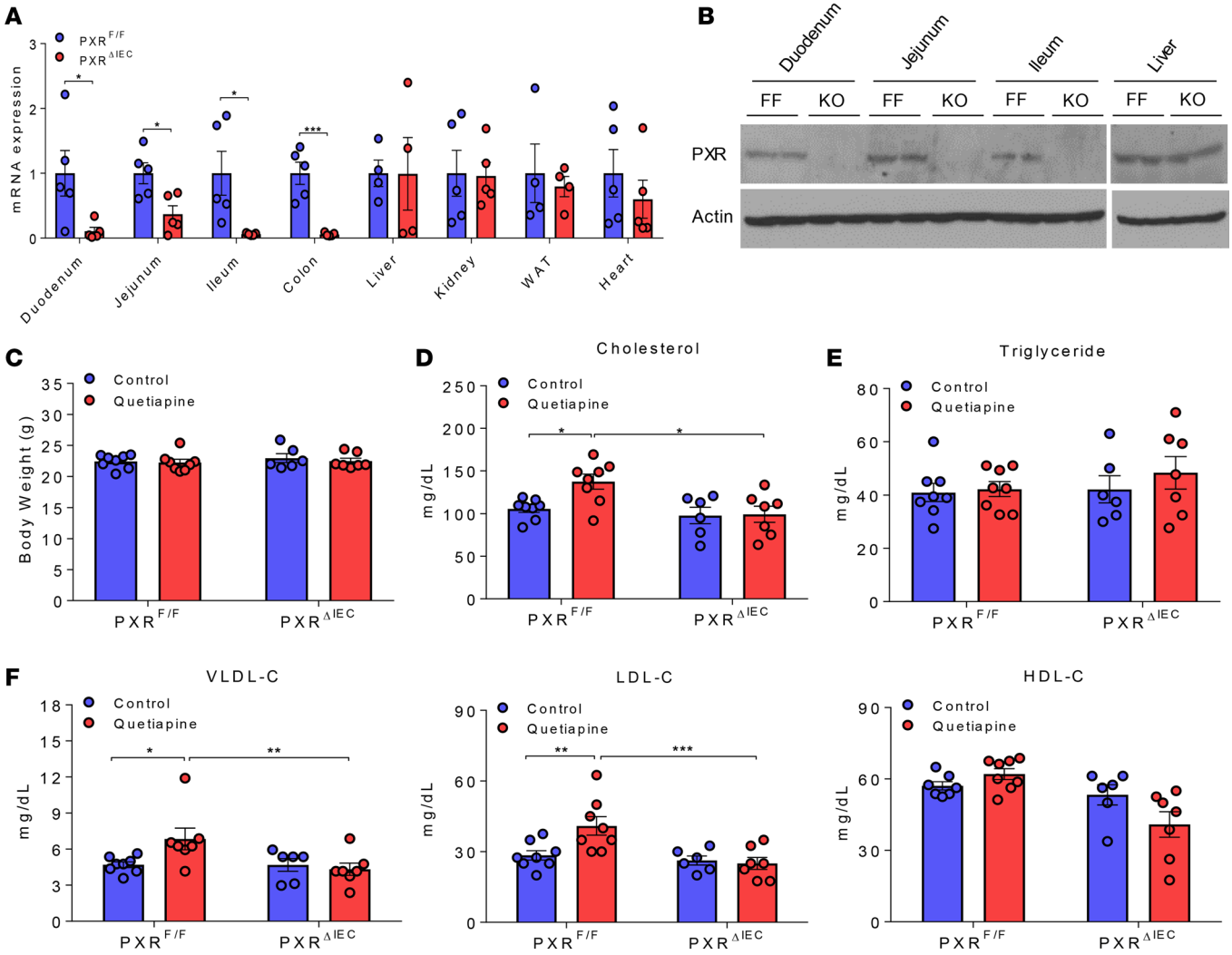

Figure 3. Quetiapine elicits hypercholesterolemia in PXR$^{fl/fl}$ mice but not in PXR$^{\Delta IEC}$ mice. (**A**) qPCR analysis of PXR mRNA levels in major tissues of PXR$^{fl/fl}$ and PXR$^{\Delta IEC}$ mice (n = 4–5, Student's t test, $^*P < 0.05$, $^{***}P < 0.001$). (**B**) Western blot analysis of PXR proteins in intestine and liver of PXR$^{fl/fl}$ and PXR$^{\Delta IEC}$ mice. (**C–F**) Eight-week-old male PXR$^{fl/fl}$ and PXR$^{\Delta IEC}$ littermates were treated with vehicle control or 10 mg/kg/day of quetiapine by oral gavage for 1 week. Body weight (**C**), fasting plasma total cholesterol (**D**), and triglyceride (**E**) levels were measured. Lipoprotein fractions (VLDL, LDL, and HDL) were isolated, and the cholesterol levels of each fraction were measured (**F**) (n = 6–8, 2-way ANOVA, $^*P < 0.05$, $^{**}P < 0.01$, and $^{***}P < 0.001$).

this DR-1 element (Figure 6B). The binding of MTP/DR-1 by PXR-RXR was specific, as excess cold probe decreased PXR-RXR binding to this element (Figure 6B). In addition, mutations of the DR-1 element were able to abolish the binding of PXR-RXR dimers to the mutant DR-1 site (Figure 6C). Two different anti-PXR antibodies also disrupted the protein-DNA complex (Figure 6C), suggesting that PXR is a component of the protein complex that binds to the MTP/DR-1 element. Next, ChIP assays demonstrated that quetiapine treatment increased the recruitment of PXR onto the MTP promotor region containing DR-1 element in the intestine of PXR$^{fl/fl}$ but not PXR$^{\Delta IEC}$ mice (Figure 6D). In addition to intestine tissue, we also used siRNA to reduce PXR expression in human intestinal LS180 cell line (Supplemental Figure 3), which has been successfully used to study PXR signaling in vitro (16, 25). Consistently, quetiapine can also promote the recruitment of PXR onto the MTP promotor in LS180 cells, but siRNA-mediated PXR knockdown reduced this recruitment (Figure 6E). Taken together, these results demonstrated that MTP is a direct transcriptional target of PXR.

Quetiapine increases intestinal lipid absorption in a PXR-dependent manner. Both NPC1L1 and MTP have been established as essential proteins mediating intestinal cholesterol absorption and transport. While NPC1L1 mediates free cholesterol uptake by enterocytes (38), MTP is required for the efficient assembly and secretion of lipoproteins (35, 36). H&E and Oil Red O staining of intestine showed that short-term

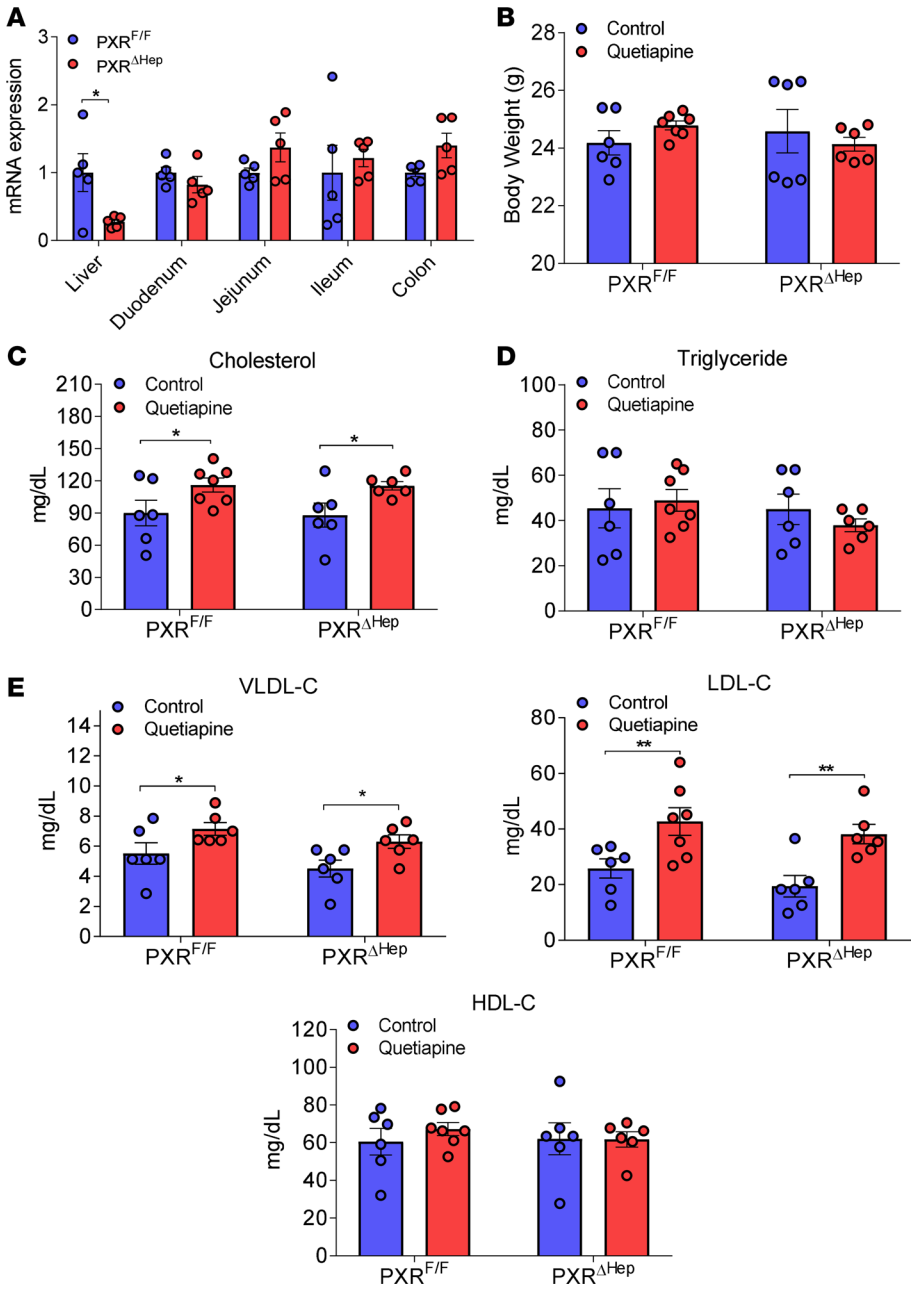

Figure 4. Quetiapine induces hypercholesterolemia in both PXR$^{fl/fl}$ and PXR$^{\Delta Hep}$ mice. (**A**) qPCR analysis of PXR mRNA levels in liver and intestine of PXR$^{fl/fl}$ and PXR$^{\Delta Hep}$ mice (n = 5, Student's t test, *P < 0.05). (**B–E**) Eight-week-old male PXR$^{fl/fl}$ and PXR$^{\Delta Hep}$ littermates were treated with vehicle control or 10 mg/kg/day of quetiapine by oral gavage for 1 week. Body weight (**B**), fasting plasma total cholesterol (**C**), and triglyceride (**D**) levels were measured. Lipoprotein fractions (VLDL, LDL, and HDL) were isolated, and the cholesterol levels of each fraction were measured (**E**) (n = 6–7, 2-way ANOVA, *P < 0.05 and **P < 0.01).

exposure to quetiapine was sufficient to increase lipid accumulation in the intestine villi of PXR$^{fl/fl}$ but not PXR$^{\Delta IEC}$ mice (Figure 7, A and B). LipidTOX immunofluorescence staining also confirmed the lipid droplet accumulation in the intestine of PXR$^{fl/fl}$ mice, and deficiency of PXR abolished the impact of quetiapine on intestinal lipid accumulation (Figure 7C). As expected, deficiency of hepatic PXR did not affect quetiapine-induced intestinal lipid accumulation (Supplemental Figure 4, A and B).

To investigate the impact of quetiapine on intestinal lipid uptake in a quantitative manner, we performed in vivo intestinal cholesterol uptake assays using [^{3}H]-cholesterol. Analysis of intestinal uptake of radiolabeled cholesterol response to oral dosing of [^{3}H]-cholesterol revealed that quetiapine treatment

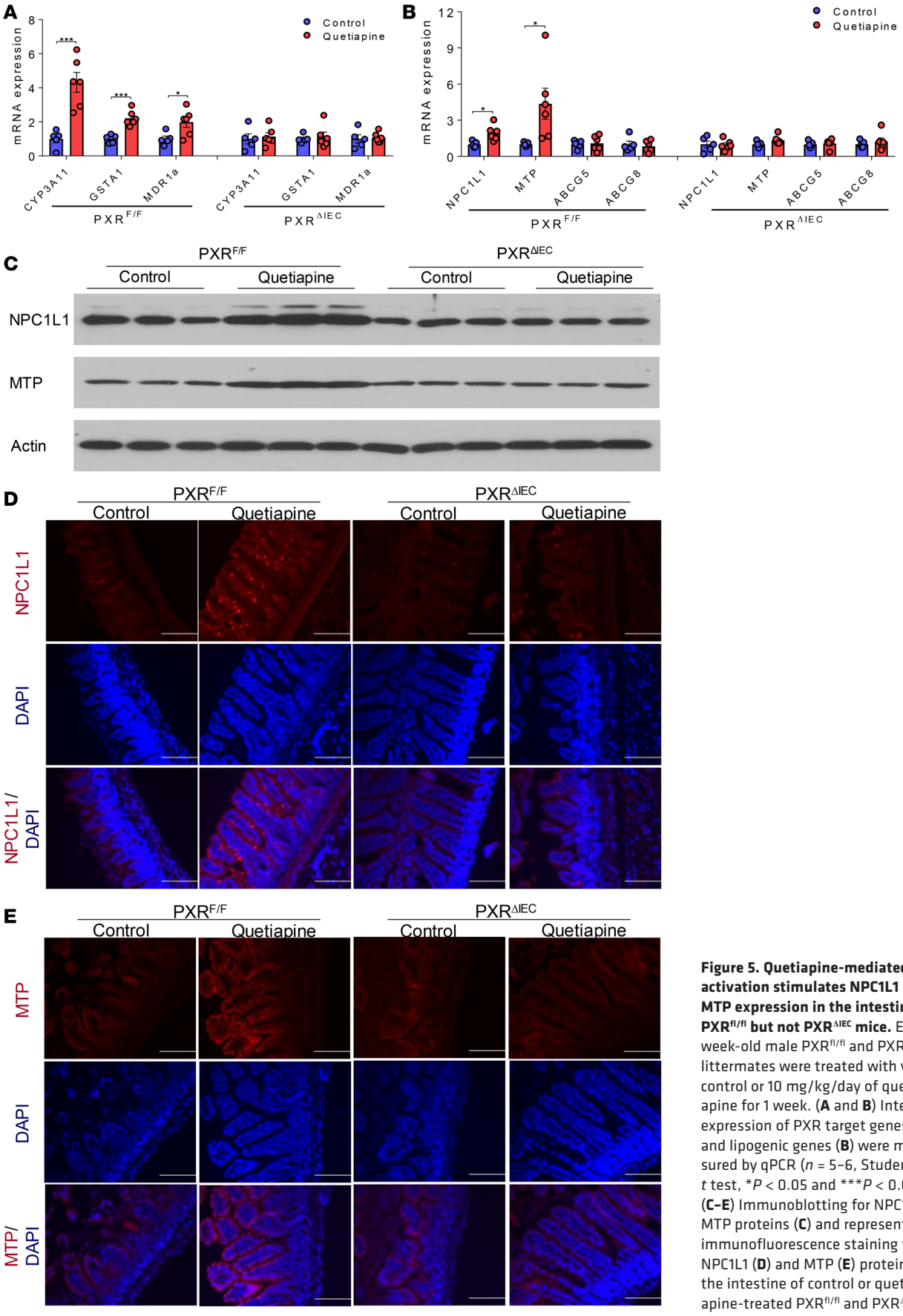

Figure 5. Quetiapine-mediated PXR activation stimulates NPC1L1 and MTP expression in the intestine of PXR$^{fl/fl}$ but not PXR$^{\Delta IEC}$ mice. Eight-week-old male PXR$^{fl/fl}$ and PXR$^{\Delta IEC}$ littermates were treated with vehicle control or 10 mg/kg/day of quetiapine for 1 week. (**A** and **B**) Intestinal expression of PXR target genes (**A**) and lipogenic genes (**B**) were measured by qPCR (n = 5–6, Student's t test, $^*P < 0.05$ and $^{***}P < 0.001$). (**C–E**) Immunoblotting for NPC1L1 and MTP proteins (**C**) and representative immunofluorescence staining for NPC1L1 (**D**) and MTP (**E**) proteins in the intestine of control or quetiapine-treated PXR$^{fl/fl}$ and PXR$^{\Delta IEC}$ mice (n = 3–5). Scale bars: 100 μM.

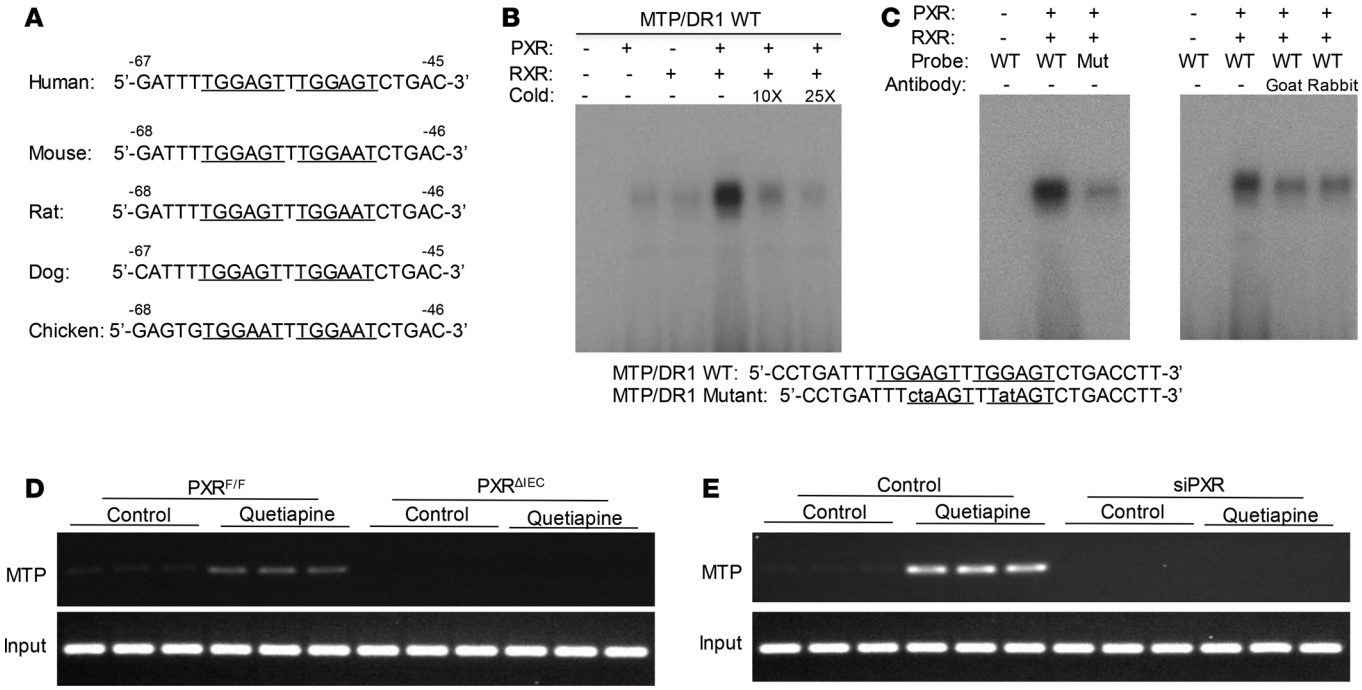

Figure 6. MTP is a transcriptional target of PXR. (**A**) Putative MTP DR-1 promoter sequences in different species. (**B** and **C**) In vitro translated human PXR and RXR proteins were incubated with [^{32}P]-labeled MTP/DR-1 probes for EMSA analysis. (**B**) PXR/RXR proteins were incubated with [^{32}P]-labeled WT MTP/DR-1 probes for EMSA analysis. (**C**) PXR/RXR proteins were incubated with [^{32}P]-labeled WT or mutated MTP/DR-1 probes for EMSA analysis (left panel). PXR/RXR proteins were incubated with 2 different anti-PXR antibodies, goat anti-PXR, or rabbit anti-PXR antibodies for 1 hour prior to the addition of the WT [^{32}P]-labeled MTP/DR-1 probes for EMSA analysis (right panel). (**D** and **E**) ChIP analysis was performed to determine the recruitment of PXR onto the MTP promoter. Intestine samples were collected from PXR$^{fl/fl}$ and PXR$^{\Delta IEC}$ mice after 1-week treatment of 10 mg/kg/day quetiapine (**D**) (n = 3). Control and PXR siRNA-treated human intestinal LS180 cells were treated with DMSO control or 10 μM quetiapine for 24 hours before ChIP analysis (**E**) (n = 3).

significantly increased cholesterol uptake in the proximal intestine of PXR$^{fl/fl}$ mice (Figure 8, A and B). Deficiency of intestinal PXR completely abolished the impact of quetiapine on cholesterol uptake in PXR$^{\Delta IEC}$ mice (Figure 8, A and B). Cholesterol absorption rates were also measured (39). The appearance of [^{3}H]-cholesterol in the plasma was nearly 2-fold greater in quetiapine-treated PXR$^{fl/fl}$ mice as compared with control mice after 6 hours following gavage of [^{3}H]-cholesterol (Figure 8C). By contrast, quetiapine did not affect the cholesterol absorption rates in PXR$^{\Delta IEC}$ mice (Figure 8C). Since MTP also plays an important role in intestinal triglyceride absorption (40), we also measured triglyceride absorption in control or quetiapine-treated mice (39). Similar to cholesterol absorption results, the appearance of [^{3}H]-triolein in the plasma was significantly greater in quetiapine-treated PXR$^{fl/fl}$ mice as compared with control mice, and quetiapine did not affect the triglyceride absorption rates in PXR$^{\Delta IEC}$ mice (Figure 8D).

It is intriguing that quetiapine treatment only increased plasma cholesterol levels but did not affect fasting plasma triglyceride levels in PXR$^{fl/fl}$ mice (Figure 3, D and E). Since plasma triglyceride levels can be affected significantly by the fasting and feeding condition (41–43), we then investigated the quetiapine's effects on plasma triglyceride under postprandial conditions (42, 44, 45). Indeed, quetiapine treatment significantly increased postprandial triglyceride and cholesterol levels in PXR$^{fl/fl}$ but not in PXR$^{\Delta IEC}$ mice following an intragastric olive oil load (Figure 8, E and F). Therefore, these results suggest that quetiapine-mediated activation of PXR stimulates intestinal lipid absorption, leading to increased hyperlipidemia in mice.

Activation of PXR by quetiapine stimulates cholesterol uptake by murine enteroids ex vivo. To further investigate the effects of quetiapine on intestinal PXR–mediated cholesterol absorption, we employed an ex vivo approach by culturing enteroids isolated from intestinal crypts of PXR$^{fl/fl}$ and PXR$^{\Delta IEC}$ mice (Figure 9A). The enteroids are considered as mini-intestines, which exhibit a similar cellular composition to and functional, region-specific aspects of the gastrointestinal epithelium (46). Consistent with the known enteroid morphology and phenotype, the enteroids we isolated also expressed CDX2 proteins, a marker for the intestine (Figure 9B) (47). We next confirmed that the expression of PXR in the enteroids from PXR$^{\Delta IEC}$ mice was significantly reduced compared with that of PXR$^{fl/fl}$ mice (Figure 9C). Consistent with the in

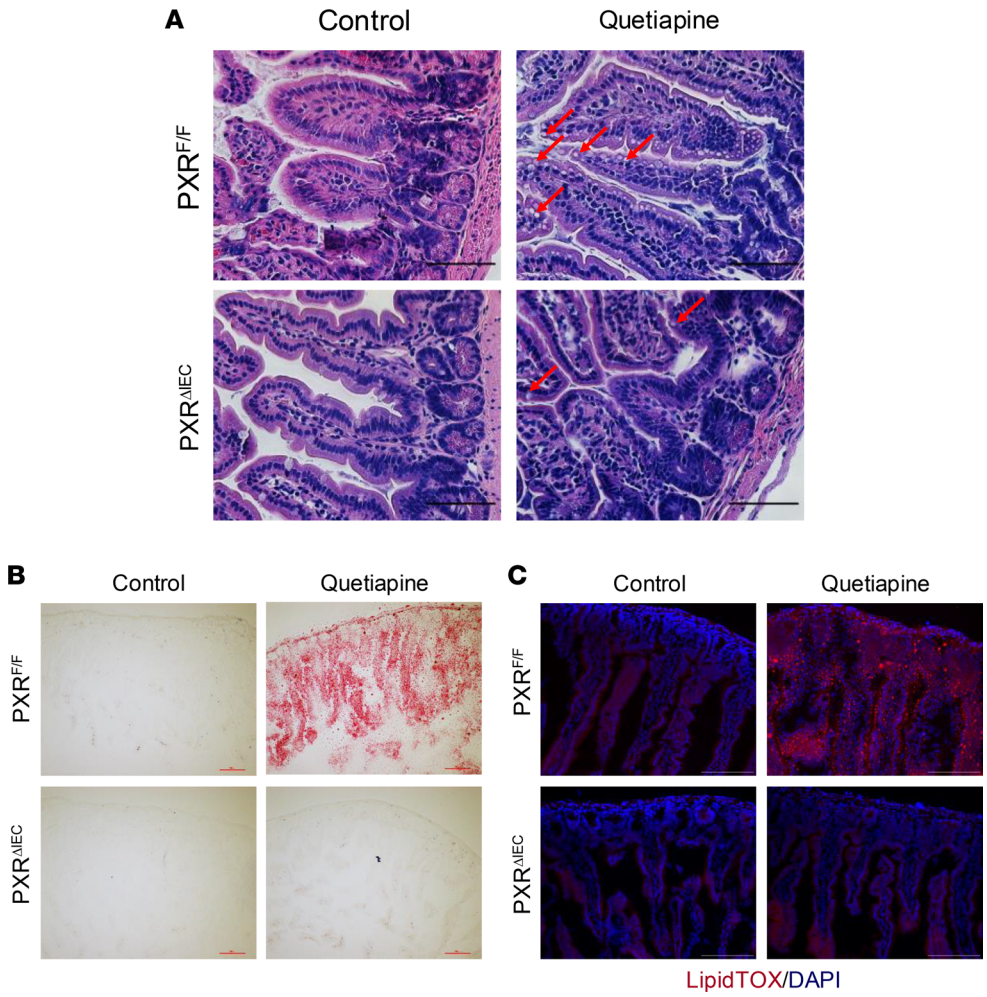

Figure 7. Quetiapine enhances lipid accumulation in the intestine of PXR$^{fl/fl}$ but not PXR$^{\Delta IEC}$ mice. Eight-week-old male PXR$^{fl/fl}$ and PXR$^{\Delta IEC}$ littermates were treated with vehicle control or 10 mg/kg/day of quetiapine for 1 week. Intestine sections were analyzed by H&E (**A**), Oil Red O (**B**), and LipidTOX immunofluorescence staining (**C**) (n = 4–5). Lipid droplets were indicated by red arrows (**A**). Scale bars: 50 μM (**A**) and 100 μM (**B** and **C**).

vivo results, quetiapine treatment also stimulated the expression of known PXR target genes, NPC1L1, and MTP in control enteroids from PXR$^{fl/fl}$ mice but not in PXR-deficient enteroids (Figure 9D). We also performed cholesterol uptake assay using micelles containing [^{3}H]-cholesterol. As expected, quetiapine treatment significantly increased uptake of [^{3}H]-cholesterol by the enteroids of PXR$^{fl/fl}$ mice but did not affect cholesterol uptake by PXR-deficient enteroids (Figure 9E). These results confirmed the important role of PXR in the regulation of intestinal cholesterol uptake.

Quetiapine stimulates NPC1L1 and MTP expression and increases cholesterol uptake in human intestinal cells. To evaluate the clinically relevant impact of quetiapine on intestinal PXR activity, hIECs were also cultured and treated with quetiapine at different doses. Quetiapine can also stimulate the expression of known hPXR target genes, NPC1L1, and MTP in hIECs in a dose-dependent manner (Figure 10A). Immunoblotting results also confirmed elevated NPC1L1 and MTP protein levels in quetiapine-treated hIECs (Figure 10B). In addition to primary hIECs, human intestinal LS180 cell lines were also used for quetiapine treatment. As expected, quetiapine treatment elevated the mRNA and protein levels of NPC1L1 and MTP in control LS180 cells (Figure 11, A and B), and siRNA-mediated PXR knockdown decreased quetiapine-mediated induction. Consistent with the results from murine enteroids, quetiapine also significantly increase [^{3}H]-cholesterol uptake by LS180 cells, which was reduced by siRNA-mediated PXR knockdown (Figure 11C). Therefore, quetiapine-mediated PXR activation can also induce NPC1L1 and MTP expression and stimulate cholesterol uptake by human intestinal cells.

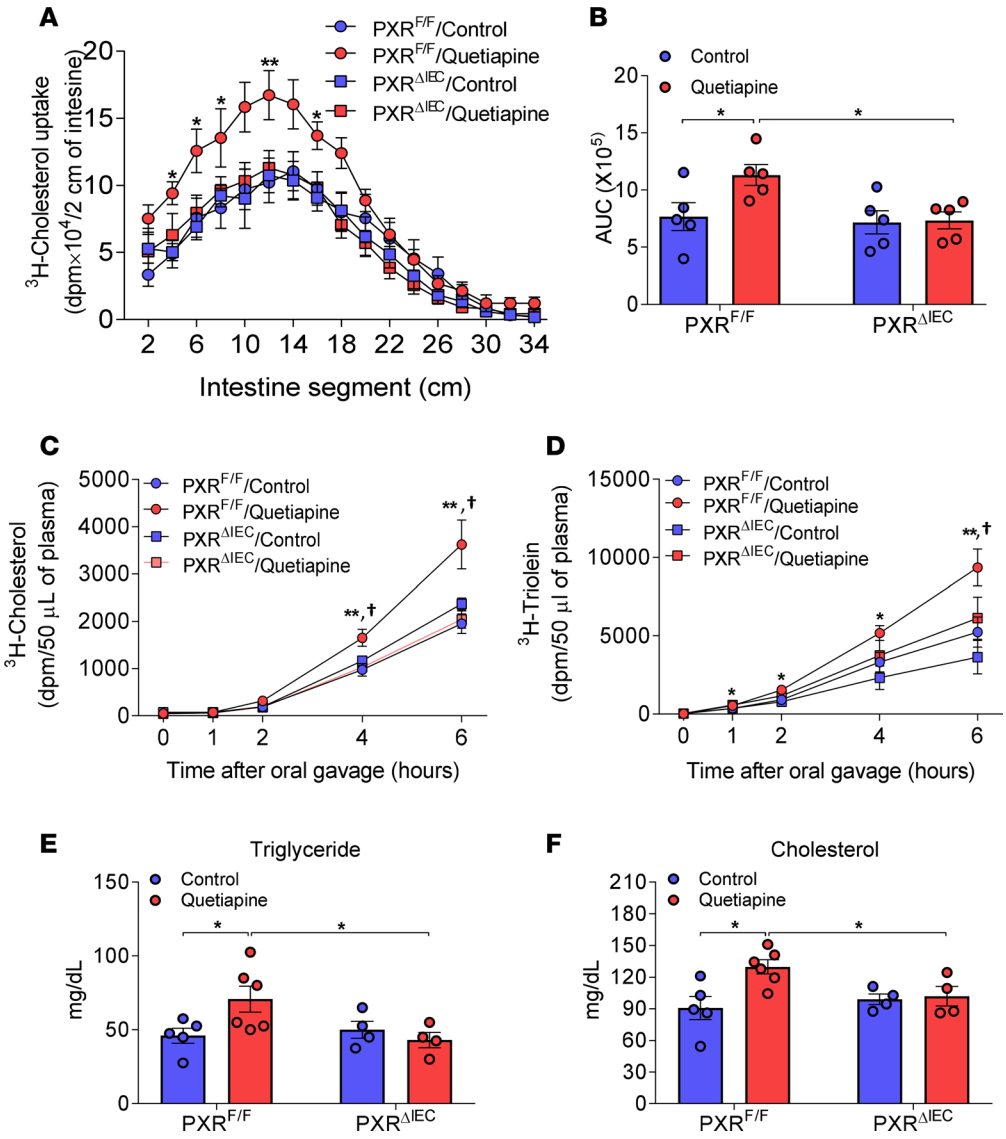

Figure 8. Quetiapine increases intestinal lipid absorption in a PXR-dependent manner. Eight-week-old male PXR$^{fl/fl}$ and PXR$^{\Delta IEC}$ littermates were treated with vehicle control or 10 mg/kg/day of quetiapine by oral gavage for 1 week. (**A** and **B**) Distribution (**A**) and AUC (**B**) of radioactivity in intestinal segments of PXR$^{fl/fl}$ and PXR$^{\Delta IEC}$ mice after an oral challenge of oil containing [^{3}H]-cholesterol for 2 hours (n = 5, 2-way ANOVA, *P < 0.05, **P < 0.01). (**C** and **D**) Cholesterol (**C**) and triglyceride (**D**) absorption rates in control or quetiapine-treated PXR$^{fl/fl}$ and PXR$^{\Delta IEC}$ mice. Mice were injected with lipase inhibitor poloxamer-407 followed by gavage with [^{3}H]-cholesterol (**C**) or [^{3}H]-triolein (**D**). Plasma samples were collected over 6 hours and measured for the presence of [^{3}H]-cholesterol or [^{3}H]-triolein (n = 3–7, 2-way ANOVA, *P < 0.05, and **P < 0.01 compared with PXR$^{fl/fl}$ mice treated with control; †P < 0.05, compared with PXR$^{\Delta IEC}$ mice treated with quetiapine). (**E** and **F**) Mice received an intragastric lipid load (10 μl/g body weight of olive oil) after 4-hour fasting. Blood samples were collected 2 hours after the lipid bolus, and postprandial plasma triglyceride (**E**) and cholesterol (**F**) levels were measured by standard methods (n = 4–6, 2-way ANOVA, *P < 0.05).

Discussion

Quetiapine is a commonly prescribed atypical antipsychotic that has been associated with increased risk of hyperlipidemia and CVD. In the current study, we identified quetiapine as a potent agonist for the nuclear receptor PXR. We then generated tissue-specific PXR-KO mice and demonstrated, for the first time to our knowledge, that quetiapine induced hyperlipidemia by targeting intestinal PXR signaling. Quetiapine-mediated PXR activation stimulated the expression of NPC1L1 and MTP, 2 key genes regulating intestinal lipid homeostasis, leading to increased intestinal lipid absorption. We further confirmed these findings in cultured murine enteroids and human intestinal cells. In addition to quetiapine, we also tested another widely used antipsychotic aripiprazole for PXR activation and found that aripiprazole did not affect either

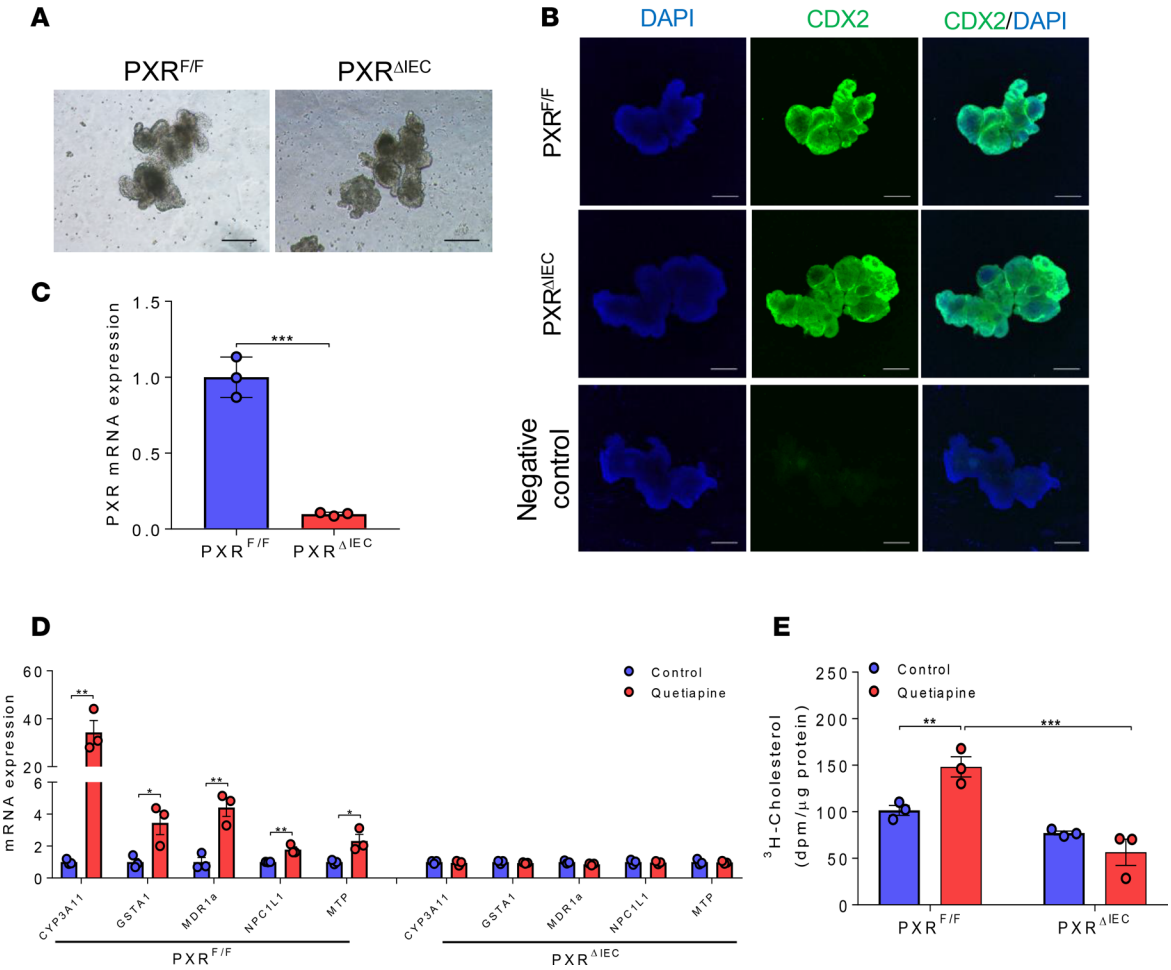

Figure 9. Activation of PXR by quetiapine stimulates cholesterol uptake by murine enteroids ex vivo. (**A** and **B**) Gross observation (**A**) and immunofluorescence staining of enteroids for CDX2 (**B**) isolated from PXR$^{fl/fl}$ and PXR$^{\Delta IEC}$ mice (n = 3). Scale bars: 200 μM. (**C**) PXR gene expression in enteroids isolated from PXR$^{fl/fl}$ and PXR$^{\Delta IEC}$ mice (n = 3, Student's t test, ***P < 0.001). (**D** and **E**) Enteroids isolated from PXR$^{fl/fl}$ or PXR$^{\Delta IEC}$ mice were treated with DMSO control or 10 μM quetiapine for 24 hours. Gene expression was analyzed by qPCR (**D**) (n = 3, Student's t test, *P < 0.05 and **P < 0.01). Enteroids were also incubated with micelle containing [^{3}H]-cholesterol for 1 hour. The radioactivity in the cells were measured (**E**) (n = 3, 2-way ANOVA, **P < 0.01 and ***P < 0.001).

mouse or human PXR activities. Interestingly, aripiprazole has been shown to have low risk of hyperlipidemia and CVD, and switching from quetiapine to aripiprazole has been demonstrated to substantially reduce CVD risk in patients (10). Therefore, these results suggest a potential role of PXR in mediating adverse effects of quetiapine in humans, which provides mechanistic insights of certain atypical antipsychotic-associated dyslipidemia and CVD.

The important role of PXR in xenobiotic metabolism has been well recognized. Recent studies have revealed potentially novel functions of PXR beyond xenobiotic metabolism, and PXR signaling has been implicated in lipid homeostasis (18). For example, we previously reported that chronic activation of PXR by feeding mice the potent PXR ligand PCN led to increased plasma total, VLDL, and LDL cholesterol levels in WT mice, but not in PXR$^{-/-}$ mice (21). Activation of PXR can also increase plasma total cholesterol and VLDL levels in apolipoprotein E*3-Leiden (ApoE*3-Leiden) mice, which have a human-like lipoprotein distribution pattern (22). In the current study, mice were treated with 10 mg/kg/day quetiapine to investigate its potential impact on lipid homeostasis. For mouse treatment, the drug doses were usually selected based on an interspecies scaling factor of 12.3 between mice and humans (33, 34), which reflects the 12.3-fold difference in surface area–to-BW ratio between mice (0.0066 m^2/0.02 kg) and humans (1.6 m^2/60 kg) (33, 34, 48). Thus, 12.3 times more drug is required in mice to be comparable with the dose in humans. The 10 mg/kg/day quetiapine dose we used in this study to treat mice is comparable with ~49 mg/day for patients with 60 kg BW, which is within or below the clinically used dose range. Therefore, we

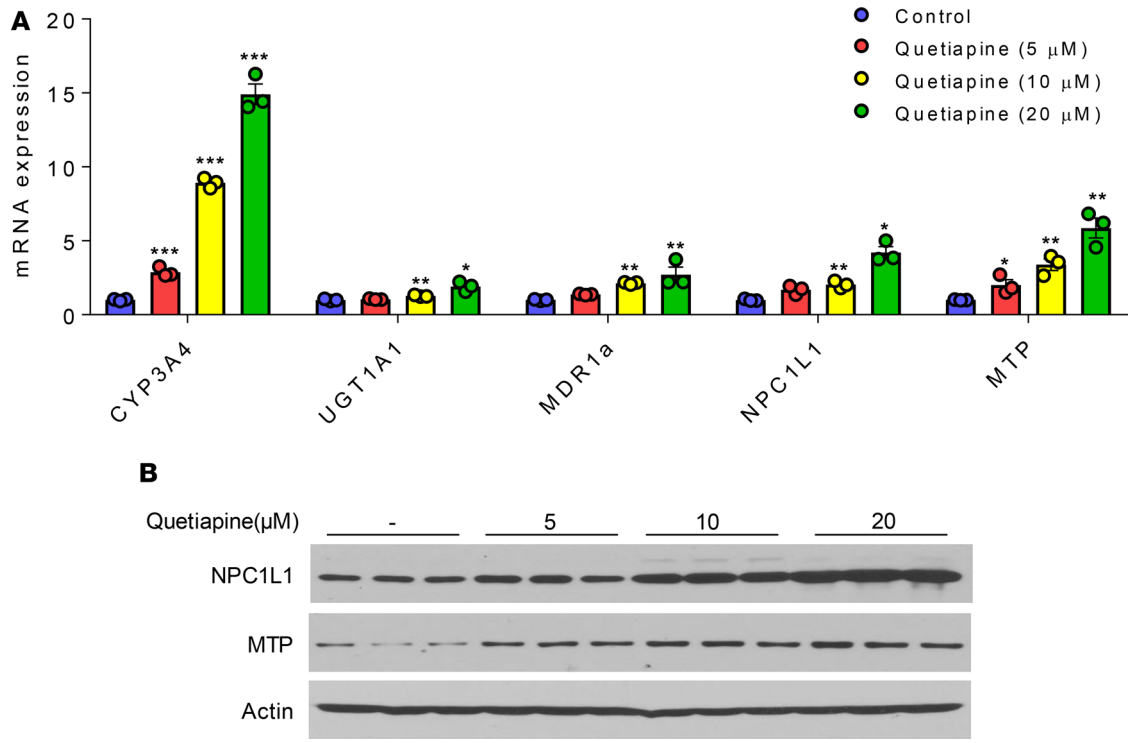

Figure 10. Quetiapine dose-dependently stimulates NPC1L1 and MTP expression in human primary intestinal epithelial cells. Human primary intestinal epithelial cells were treated with DMSO control or 5, 10, or 20 μM quetiapine for 24 hours. (**A**) The expressional levels of known PXR target genes, NPC1L1, and MTP were analyzed by qPCR (n = 3, 1-way ANOVA, $^{*}P < 0.05$, $^{**}P < 0.01$, and $^{***}P < 0.001$ compared with control group). (**B**) Immunoblotting analysis of NPC1L1 and MTP proteins (n = 3).

chose the 10 mg/kg/day dose for short-term quetiapine treatment in mice and found that only the 1-week treatment led to significantly increased plasma total, VLDL, and LDL cholesterol levels in control mice.

While activation of PXR has been reported to affect lipogenic gene expression in both liver and intestine, results from our PXR–conditional KO mice concluded that deficiency of PXR in the intestine but not in the liver abolished the quetiapine's hyperlipidemic effects. Intestinal lipid transportation plays a central role in maintaining whole-body lipid homeostasis, and previous studies by us and others have indicated a potential role of PXR in intestinal lipid homeostasis; however, the underlying mechanisms were not completely understood (18, 24, 25). In addition to prototypic PXR target genes such as CYP3A11 and MDR1a, quetiapine-mediated PXR activation significantly increased the expression of NPC1L1 and MTP, 2 key lipogenic genes in intestine. NPC1L1 is an essential transporter in mediating intestinal cholesterol uptake (35, 38, 49). We previously identified NPC1L1 as a direct transcriptional target of PXR and also demonstrated that activation of PXR can increase cholesterol uptake by intestinal cells in vitro (25). However, the impact of PXR agonists on intestinal cholesterol uptake and absorption in vivo has not been investigated. In the present study, we found that quetiapine-mediated PXR activation can indeed increase intestinal cholesterol uptake and absorption in $PXR^{fl/fl}$ but not $PXR^{\Delta IEC}$ mice. Consistently, quetiapine treatment also increased NPC1L1 expression and stimulated cholesterol uptake ex vivo in cultured murine enteroids and human intestinal LS180 cells in a PXR-dependent manner. NPC1L1 mutation has been associated with reduced plasma LDL cholesterol levels and a reduced risk of CVD in clinical studies (50). NPC1L1 is also the molecular target of the clinically used cholesterol-lowering drug ezetimibe, which inhibits cholesterol absorption (38). Therefore, it is likely that PXR-stimulated NPC1L1 expression contributes to quetiapine-associated hypercholesterolemia in patients.

In addition to NPC1L1, quetiapine-mediated PXR activation also elevated the intestinal expression of MTP, which is important for lipid absorption and lipoprotein assembly (36). Consistent with the known functions of MTP (36, 40), quetiapine treatment also led to increased intestinal triglyceride absorption and elevated postprandial plasma triglyceride levels. The function of MTP in intestinal lipid homeostasis has been well studied. MTP gene variants have also been associated with plasma lipid levels in humans (51, 52).

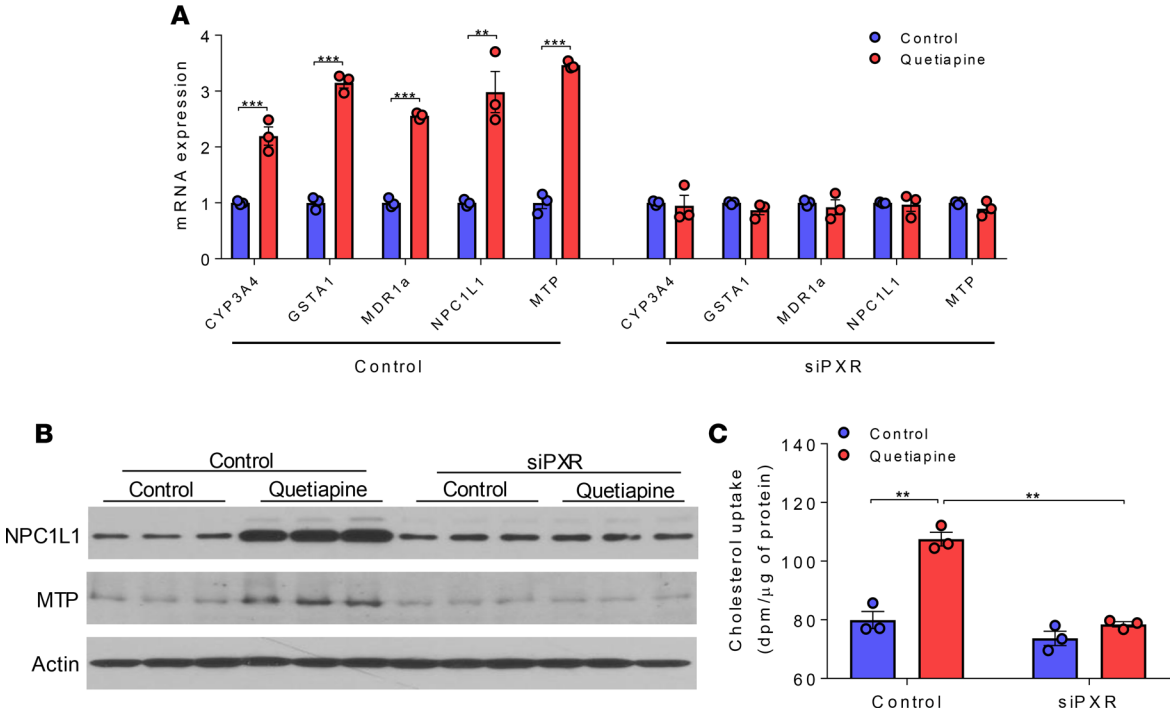

Figure 11. Quetiapine-mediated PXR activation increases NPC1L1 and MTP expression and increases cholesterol uptake in human intestinal LS180 cells. Human intestinal LS180 cells were transfected with control siRNA or siRNA against PXR (siRXR). Control or siPXR LS180 cells were treated with DMSO control or 10 μM quetiapine for 24 hours. (**A**) The expression levels of known PXR target genes, NPC1L1, and MTP were analyzed by qPCR (n = 3, Student's t-test, $^{**}P < 0.01$ and $^{***}P < 0.001$). (**B**) Immunoblotting analysis of NPC1L1 and MTP proteins in control or siPXR LS180 cells (n = 3). (**C**) Control or siPXR LS180 cells were incubated with micelle containing [^{3}H]-cholesterol for 1 hour. The radioactivity in the cells were measured (n = 3, 2-way ANOVA, $^{**}P < 0.01$).

Inhibition or deletion of MTP can lead to decreased plasma lipid levels and atherosclerosis development in mice (40, 53). By contrast, elevated intestinal MTP expression induced hyperlipidemia and atherosclerosis in mouse models (54, 55). The transcriptional regulation of MTP has not been fully understood. Interestingly, we identified a very conserved DR-1 element located in MTP promoter and also confirmed MTP as a transcriptional target of PXR by EMSA and ChIP assays. These results suggest that PXR can regulate intestinal lipid homeostasis at multiple levels, and it is possible that PXR may regulate other genes important for intestinal lipid transport and lipoprotein assembly. Future studies are required to investigate the detailed mechanisms through which PXR regulates other signaling pathways and mediates lipid homeostasis in animal models and in humans.

In summary, we demonstrated that the commonly prescribed atypical antipsychotic quetiapine is a potent PXR-selective agonist. We also generated a potentially novel intestine-specific PXR-KO mouse model and concluded that intestinal PXR signaling mediates quetiapine's dyslipidemic effects in mice. Interestingly, quetiapine-mediated PXR activation stimulated the expression of the key intestinal genes essential for lipid homeostasis including, NPC1L1 and MTP, leading to increased intestinal lipid absorption. While NPC1L1 is a known PXR target gene, we identified a conserved DR-1–type PXR-response element in the MTP promoter and established MTP as a direct transcriptional target of PXR. Findings from this study may stimulate further investigations of atypical antipsychotic-associated dyslipidemia and CVD risk, the mechanisms by which quetiapine and other drugs activate PXR, and the potentially complex functions of PXR in lipid homeostasis.

Methods

Animals. Mice carrying PXR flox alleles ($PXR^{fl/fl}$) on C57BL/6 background were generated by using mouse embryonic stem cell clones containing conditional PXR flox allele from International Knockout Mouse Consortium (EUMMCR, EPD0141_1_G04) (29). $PXR^{fl/fl}$ mice were further crossed with Villin-Cre (The Jackson Laboratory; catalog 004586) or Albumin-Cre transgenic mice (The Jackson Laboratory; catalog 003574) to generate $PXR^{\Delta IEC}$ or $PXR^{\Delta Hep}$. $PXR^{fl/fl}$, $PXR^{\Delta IEC}$, and $PXR^{\Delta Hep}$ mice used in this study had the same background (PXR flox alleles) except for 1 allele of $PXR^{\Delta IEC}$ and $PXR^{\Delta Hep}$ mice carrying Villin-Cre

and Albumin-Cre, respectively. All experiments using $PXR^{\Delta IEC}$ and $PXR^{\Delta Hep}$ mice in this study also included their corresponding $PXR^{fl/fl}$ littermates as controls. For the treatment, 8-week-old male mice were fed a semisynthetic low-fat AIN76 diet containing 4.2% fat and 0.02% cholesterol (Research Diet; D00110804C) (16, 21, 25) and were treated by oral gavage with vehicle (corn oil; MilliporeSigma, C8267) or 10 mg/kg BW of quetiapine daily for 1 week. On the day of euthanasia, mice were fasted for 6 hours following the dark cycle (feeding cycle), and blood and tissues were then collected as previously described (16, 21, 56).

Reagents and plasmids. Quetiapine (PHR1856), aripiprazole (SML0935), pregnenolone 16α-carbonitrile (P0543), and rifampicin (R7382) were purchased from MilliporeSigma. All the chemicals were dissolved in DMSO. All the plasmids used in this study have been described before (16, 25, 26), including human and mouse PXR expression vectors: GAL4 DNA-binding domain–linked (DBD-linked) nuclear receptor LBD vectors; VP16-hPXR; GAL4 DBD–linked nuclear receptor coregulators (SRC-1, PBP, NCoR, and SMRT), PXR-dependent CYP3A4 promoter reporter (CYP3A4XREM-luciferase), CYP3A2 promoter reporter ($[CYP3A2]_3$-luciferase), GAL4 reporter (MH100-luciferase), and CMX–β-galactosidase expression vector (16, 25, 26).

Cell culture and transfection assay. The human hepatic cell line HepG2 (ATCC HB-8065) and intestine epithelial cell line LS180 (ATCC CL-187) were obtained from the American Type Culture Collection. Transfection assays were performed as described previously (26, 27, 57). Briefly, the cells were transfected with various expression plasmids, as well as the corresponding luciferase reporter plasmids, together with cytomegalovirus X–β-galactosidase control plasmids using FuGENE 6 (Promega Corporation; E2691). The cells were then incubated with the corresponding ligands — as indicated in the figure legends — overnight, and β-galactosidase and luciferase assays were performed as described (26, 27). Fold activation was calculated relative to the solvent controls. EC_{50} values were calculated by curve fitting of data, using Prism software. For the mammalian 2-hybrid assays, HepG2 cells were transfected with GAL4 reporter, VP16-hPXR, and coregulator plasmids including GAL4-SRC1, GAL4-PBP, GAL4-NCoR, and GAL4-SMRT (26, 27). The cells were then treated with compounds at the indicated concentrations.

Competitive ligand-binding assay. LanthaScreen TR-FRET PXR competitive binding assays were conducted according to the manufacturer's protocol as previously described (58). Briefly, assays were performed in a volume of 20 μl in 384-well solid black plates with 5 nM GST-hPXR LBD (PXR-LBD [GST]; Invitrogen; PV4840), 40 nM fluorescent-labeled hPXR agonist (fluomore PXR green; Invitrogen; PV4843), 5 nM terbium-labeled anti-GST antibody (LanthaScreen Tb anti-GST antibody; Invitrogen; PV3550), and test compounds at different concentrations. The reaction mixture was incubated at 25°C for 1 hour. The terbium emission peak was then measured at 490 nm, while the fluorescein emission was measured at 520 nm by a Synergy H1 Hybrid Reader (BioTek Instruments Inc.). The TR-FRET ratio was calculated and expressed as the signal from the fluorescein emission divided by the terbium signal.

Plasma analysis. Plasma total cholesterol and triglyceride concentrations were determined enzymatically by colorimetric methods as described previously (Wako; cholesterol 999-02601 and triglyceride 994-02891) (16, 21, 56). The lipoprotein fractions were isolated by spinning 60 μl of plasma in a TL-100 ultracentrifuge (Beckman Coulter) as described previously (16, 21). The cholesterol content of each supernatant and the final infranatant were measured and taken to be VLDL (<1.006 g/ml), LDL (1.006 ≤ density [d] ≤ 1.063 g/ml), and high-density lipoprotein (HDL) (d >1.063 g/ml) cholesterol. Cholesterol concentrations in all 3 fractions were then determined enzymatically by the same colorimetric method (16, 21, 56).

Postprandial triglyceride response. Postprandial triglyceride response was conducted as described previously (45). After 1-week treatment of quetiapine, the mice were fasted for 4 hours and received an intragastric load of 10 μl/g BW olive oil (MilliporeSigma, O1514). Blood samples were drawn by cardiac puncture 2 hours after the lipid bolus. Plasma triglyceride and cholesterol levels were determined by the same colorimetric method as mentioned above.

In vivo lipid uptake and absorption assays. The intestinal cholesterol uptake was examined as previously described (59, 60). Mice were fasted for 4 hours and gavaged with 200 μl of corn oil containing 2 μCi of [^{3}H]-cholesterol (PerkinElmer; NET139001MC). Two hours later, the small intestine (between the base of the stomach and the cecal junction) were excised, flushed with 0.5 mM sodium taurocholate (MilliporeSigma, S0900000), and cut into 2-cm segments. Segments were incubated with 500 μl of 1 N NaOH (MilliporeSigma, S8045) overnight at 65°C and mixed with ScintiSafe (Thermo Fisher Scientific; 6196-95-8) for scintillation counting. In vivo intestinal cholesterol or triglyceride absorption was also determined following the protocol previously described (39, 45). Mice were fasted for 4 hours and gavaged with corn oil containing 2 μCi

of [^{3}H]-cholesterol (PerkinElmer; NET139001MC) or 2 μCi of [^{3}H]-Triolein (PerkinElmer; NET431001MC), immediately followed by i.p. injection with lipoprotein lipase inhibitor poloxamer-407 (MilliporeSigma; 16758) (1 g/kg BW). Blood was then collected by retro-orbital bleeding under isoflurane anesthesia over 6 hours, and plasma [^{3}H]-cholesterol or [^{3}H]-Triolein was measured by liquid scintillation counting.

Enteroid culture and cholesterol uptake assay. Primary crypts were isolated as previously described with modifications (61). $PXR^{fl/fl}$ or $PXR^{\Delta IEC}$ mice were euthanized, and 8 cm of intestine was collected at the position of 3-cm distally away from stomach to avoid Brunner's gland reside. The separated intestine was then flushed twice with DPBS and incubated with cold DPBS on ice for 1 hour. The intestine was cut longitudinally and minced into 1-cm pieces, washed with cold DPBS on a rocker for 5 minutes at 4°C, and placed in chelation buffer (DPBS with 2 mM EDTA; MilliporeSigma, 34103) on a rocker for 30 minutes at 4°C. To dissociate individual crypts, chelation buffer was replaced by shaking buffer (DPBS with 1 % of sorbital [MilliporeSigma, 240850] and 1% of sucrose [MilliporeSigma, S7903]) for 1 minute with shaking by hand. Total 500 crypts were placed into 50 μl of depolymerized Matrigel (Corning; catalog 354248) containing 250 ng of R-Spondin 1 (R&D Systems, 3474-RS-050), 50 ng of Noggin (R&D Systems, 1967-NG-025/CF), and 25 ng of EGF (R&D Systems, 2028-EG-200). The Matrigel and crypts suspensions were then incubated with 500 μl of minigut culture media (advanced DMEM/F12, Thermo Fisher Scientific, 12634010; containing 1 % of L-glutamine [MilliporeSigma, 59202C], 1 % of penicillin-streptomycin [MilliporeSigma, P4333], 10 mM HEPES [Invitrogen, 15630-106], 1 % of N_2 supplement [Invitrogen, 17502048], and 2 % of B27 supplement [Invitrogen, 17504044]) in a 24-well plate for 1 day at 37°C in a 5 % CO_2 incubator. The media was replaced with enteroid growth media (minigut media containing 250 ng of R-Spondin 1, 50 ng of Noggin, and 25 ng of EGF) every 3 days until the enteroids were mature. The mature enteroids were treated with minigut media containing 20 μM of quetiapine or vehicle for 24 hours. After depolymerized with ice cold DPBS, Matrigel was removed from enteroids by washing with ice cold PBS. The morphology of matured enteroids was photographed by optical microscope (Nikon ECLIPSE 55i). Immunofluorescence staining of fixed enteroids for CDX2 (1:100 dilution; Abcam; catalog ab76541) was conducted and photographed by confocal microscope (Nikon ECLIPSE Ti). The total RNAs were extracted from enteroids for quantitative PCR (qPCR) analysis. Cholesterol uptake assay was performed as previous described (25). Briefly, micelles were prepared as previously described (25), and 1 μCi of [^{3}H]-cholesterol (PerkinElmer; NET139001MC) per μmol of cholesterol was added to the organic lipid solution before evaporating under a mild stream of Argon. The lipid film was hydrated in serum-free MEM (MilliporeSigma, 56419C) containing 0.5% fatty acid-free BSA (MilliporeSigma; 9048-46-8) and incubated at 37°C in a rotating incubator. Solutions were filtered through a 0.45-μm Surfactant-Free Cellulose Acetate filter (Corning; 431220). Enteroids were incubated with micelle containing [^{3}H]-cholesterol (PerkinElmer; NET139001MC) for 1 hour at 37°C in a 5 % CO_2 incubator. Enteroids were then washed with cold PBS twice and lysed with 500 μl of 0.1 N NaOH. The radioactivity was measured by liquid scintillation counting and normalized to total protein mass.

hIEC culture and treatment. hIECs (Lonza Group; cc-2931) and optimized culture media were purchased from Lonza Group. hIECs are primary cells representing both villi (enterocytes, goblet, and enteroendocrine cells) and crypts structures. After 5-day culture, the cells were treated with quetiapine at the doses of 5, 10, and 20 μM for 24 hours. Then, the total RNA and protein were extracted for qPCR and Western blotting analysis, respectively.

Histological analysis. For H&E staining, tissues were fixed in 4% neutral buffered formalin (Thermo Fisher Scientific, 22-046-361) and embedded in paraffin. Tissue sections were stained with hematoxylin (MilliporeSigma; 1.05175) and eosin (MilliporeSigma; R03040) following standard protocols. Oil Red O staining of neutral lipids was performed as previously described (56, 62). In brief, intestine tissues were embedded in OCT (SAKURA, 4583) and sectioned at 10 μm. Tissue sections were then dried, fixed in 4% PFA (MilliporeSigma, P6148), incubated for 5 minutes in 60% isopropanol (Thermo Fisher Scientific, A426P-4), and then incubation in 0.3% Oil Red O (MilliporeSigma; O0625) for 20 minutes.

RNA isolation and qPCR analysis. Total RNA was isolated from mouse tissues or cells using TRIzol Reagent (Thermo Fisher Scientific; 15596026), and qPCR was performed using gene-specific primers and the SYBR Green PCR kit (Bio-Rad; 170-8886) as previously described (25, 63). The sequences of primer sets used in this study are listed in Supplemental Table 1.

Western blotting. Western blotting was also performed as previously described (62, 64, 65). Proteins were extracted from animal tissues or cells, quantified with the Bradford assay (Thermo Fisher Scientific; 23225), and subjected to SDS-PAGE on 8-12% gels. The proteins were electrophoretically

transferred from the gel to a nitrocellulose membrane, which was blocked with blocking buffer (1× PBS with 0.1% Tween-20 and 5% nonfat dry milk) for 1 hour at room temperature and then incubated with blocking buffer containing anti-PXR (1:500 dilution; Santa Cruz Biotechnology Inc.; catalog sc-7739), anti-NPC1L1 (1:1000 dilution; Novus Biologicals; catalog NB400-128), anti-MTP (1:1000 dilution; Santa Cruz Biotechnology Inc.; catalog sc-33316), or anti-actin (1:5000 dilution; MilliporeSigma; catalog A2066) antibodies overnight at 4°C. The membranes were incubated with HRP-conjugated secondary antibodies with blocking buffer at room temperature for 1 hour and were developed with an ECL system (Thermo Fisher Scientific; catalog 32209).

ChIP. ChIP analysis was performed by using a SimpleChIP Enzymatic Chromatin IP Kit (Cell Signaling Technology; 9003) as previously described (25). Anti-PXR antibodies (Santa Cruz Biotechnology Inc.; catalog sc-25381) were utilized in the ChIP assay. The precipitated genomic DNA was purified using spin column purification kit (Cell Signaling Technology; 14209), followed by qPCR analysis with the primers targeting the PXR response element in the MTP promoter.

EMSA. EMSA was performed as previously described (25, 56). Briefly, human MTP/DR1 probe (5′-CCTGATTTTGGAGTTTGGAGTCTGACCTT-3′) and mutated MTP/DR1 probe (5′-CCTGATTTctaAGTTTatAGTCTGACCTT-3′) were generated by annealing the oligonucleotides to the complementary strand. Double-stranded oligonucleotides were end-labeled using T4 polynucleotide kinase (New England Biosciences; M0201S) and γ-[^{32}P]-ATP (PerkinElmer; NEG002A100UC). Then, 5 μl of in vitro-translated PXR or RXR protein by TnT T7 Quick Coupled Transcription/Translation System (Promega; L1170) was incubated with 2 μg of poly d(I-C) (MilliporeSigma, 10108812001), 2 μl of bandshift buffer (50 mM $MgCl_2$ [MilliporeSigma, M8266] and 340 mM KCl [MilliporeSigma, P9333]), and 6 μl of delta buffer (0.1 mM EDTA, 40 mM KCl, 25 mM HEPES [pH 7.6], 8% Ficoll 400 [MilliporeSigma, F2637], and 1 mM dithiothreitol [MilliporeSigma, D0632]) on ice for 10 minutes, followed by another 30-minute incubation with [^{32}P]-labeled double-stranded oligonucleotide probe (100,000 cpm) on ice. For the supershift assay, proteins were incubated with 2 μg of goat anti-PXR (Santa Cruz Biotechnology Inc.; catalog sc-7739) or rabbit anti-PXR (Santa Cruz Biotechnology Inc.; catalog sc-25381) antibodies for 1 hour prior to incubation with [^{32}P]-labeled probe. The binding complexes were subjected to electrophoresis in a 6% nondenaturing polyacrylamide gel containing 0.5 × Tris-borate EDTA (TBE; MilliporeSigma, 93290) buffer. The gels were dried and visualized by exposure to X-ray film (Thermo Fisher Scientific; 34089).

Statistics. All data are presented as the mean ± SEM. Individual pairwise comparisons were analyzed by 2-sample, 2-tailed Student's *t* tests unless otherwise noted, with $P < 0.05$ was regarded as significant. One-way ANOVA was used when multiple comparisons were made, followed by Dunnett's test for multiple comparisons to a control. Two-way ANOVA was used when multiple comparisons were made followed by a Bonferroni multiple comparisons test. Two-way ANOVA was done using SigmaPlot 13.0. The other statistics were analyzed using GraphPad Prism.

Study approval. All animal studies were performed in compliance with the IACUC protocol approved by the University of Kentucky.

Author contributions

CZ, ZM, YS, and XZ conceptualized and designed the research. ZM and TG performed most of the experiments and analyzed the data, with the help from YS and SHP. CZ, ZM, TG, and XZ wrote the manuscript.

Acknowledgments

The authors would like to thank all the lab members for the technique assistant and Chingwen Yang at Rockefeller University for the help with PXR-flox mouse generation. This work was supported by NIH grants, R01HL123358, R01ES023470, R01HL131925, and R21ES022745 (to CZ). The authors also acknowledge the core services (supported by NIH grant P30GM127211).

Address correspondence to: Changcheng Zhou, Department of Pharmacology and Nutritional Sciences, University of Kentucky, 900 South Limestone, 517 Wethington Building, Lexington, Kentucky 40536, USA. Phone: 859.218.1801; Email: c.zhou@uky.edu.

1. Keating GM, Robinson DM. Quetiapine: a review of its use in the treatment of bipolar depression. *Drugs*. 2007;67(7):1077–1095.
2. Bowden CL, et al. A randomized, double-blind, placebo-controlled efficacy and safety study of quetiapine or lithium as monotherapy for mania in bipolar disorder. *J Clin Psychiatry*. 2005;66(1):111–121.
3. Soeiro-DE-Souza MG, et al. Role of quetiapine beyond its clinical efficacy in bipolar disorder: From neuroprotection to the treatment of psychiatric disorders (Review). *Exp Ther Med*. 2015;9(3):643–652.
4. Thase ME, et al. Efficacy of quetiapine monotherapy in bipolar I and II depression: a double-blind, placebo-controlled study (the BOLDER II study). *J Clin Psychopharmacol*. 2006;26(6):600–609.
5. Vieta E, et al. Bipolar disorders. *Nat Rev Dis Primers*. 2018;4:18008.
6. Asmal L, Flegar SJ, Wang J, Rummel-Kluge C, Komossa K, Leucht S. Quetiapine versus other atypical antipsychotics for schizophrenia. *Cochrane Database Syst Rev*. 2013;(11):CD006625.
7. Wetterling T. Bodyweight gain with atypical antipsychotics. A comparative review. *Drug Saf*. 2001;24(1):59–73.
8. Meyer JM, Koro CE. The effects of antipsychotic therapy on serum lipids: a comprehensive review. *Schizophr Res*. 2004;70(1):1–17.
9. Daumit GL, et al. Antipsychotic effects on estimated 10-year coronary heart disease risk in the CATIE schizophrenia study. *Schizophr Res*. 2008;105(1-3):175–187.
10. Stroup TS, et al. Effects of switching from olanzapine, quetiapine, and risperidone to aripiprazole on 10-year coronary heart disease risk and metabolic syndrome status: results from a randomized controlled trial. *Schizophr Res*. 2013;146(1-3):190–195.
11. Olfson M, Marcus SC, Corey-Lisle P, Tuomari AV, Hines P, L'Italien GJ. Hyperlipidemia following treatment with antipsychotic medications. *Am J Psychiatry*. 2006;163(10):1821–1825.
12. de Leon J, et al. A clinical study of the association of antipsychotics with hyperlipidemia. *Schizophr Res*. 2007;92(1-3):95–102.
13. Vázquez-Bourgon J, Pérez-Iglesias R, Ortiz-García de la Foz V, Suárez Pinilla P, Díaz Martínez Á, Crespo-Facorro B. Long-term metabolic effects of aripiprazole, ziprasidone and quetiapine: a pragmatic clinical trial in drug-naïve patients with a first-episode of non-affective psychosis. *Psychopharmacology (Berl)*. 2018;235(1):245–255.
14. Blumberg B, et al. SXR, a novel steroid and xenobiotic-sensing nuclear receptor. *Genes Dev*. 1998;12(20):3195–3205.
15. Dussault I, Lin M, Hollister K, Wang EH, Synold TW, Forman BM. Peptide mimetic HIV protease inhibitors are ligands for the orphan receptor SXR. *J Biol Chem*. 2001;276(36):33309–33312.
16. Helsley RN, Sui Y, Ai N, Park SH, Welsh WJ, Zhou C. Pregnane X receptor mediates dyslipidemia induced by the HIV protease inhibitor amprenavir in mice. *Mol Pharmacol*. 2013;83(6):1190–1199.
17. Kliewer SA, Goodwin B, Willson TM. The nuclear pregnane X receptor: a key regulator of xenobiotic metabolism. *Endocr Rev*. 2002;23(5):687–702.
18. Zhou C. Novel functions of PXR in cardiometabolic disease. *Biochim Biophys Acta*. 2016;1859(9):1112–1120.
19. Zhou C, Verma S, Blumberg B. The steroid and xenobiotic receptor (SXR), beyond xenobiotic metabolism. *Nucl Recept Signal*. 2009;7:e001.
20. Kliewer SA. Nuclear receptor PXR: discovery of a pharmaceutical anti-target. *J Clin Invest*. 2015;125(4):1388–1389.
21. Zhou C, King N, Chen KY, Breslow JL. Activation of PXR induces hypercholesterolemia in wild-type and accelerates atherosclerosis in apoE deficient mice. *J Lipid Res*. 2009;50(10):2004–2013.
22. de Haan W, et al. PXR agonism decreases plasma HDL levels in ApoE3-Leiden.CETP mice. *Biochim Biophys Acta*. 2009;1791(3):191–197.
23. Zhou J, et al. A novel pregnane X receptor-mediated and sterol regulatory element-binding protein-independent lipogenic pathway. *J Biol Chem*. 2006;281(21):15013–15020.
24. Cheng J, Krausz KW, Tanaka N, Gonzalez FJ. Chronic exposure to rifaximin causes hepatic steatosis in pregnane X receptor-humanized mice. *Toxicol Sci*. 2012;129(2):456–468.
25. Sui Y, Helsley RN, Park SH, Song X, Liu Z, Zhou C. Intestinal pregnane X receptor links xenobiotic exposure and hypercholesterolemia. *Mol Endocrinol*. 2015;29(5):765–776.
26. Sui Y, et al. Bisphenol A and its analogues activate human pregnane X receptor. *Environ Health Perspect*. 2012;120(3):399–405.
27. Zhou C, et al. The dietary isothiocyanate sulforaphane is an antagonist of the human steroid and xenobiotic nuclear receptor. *Mol Pharmacol*. 2007;71(1):220–229.
28. Glass CK, Rosenfeld MG. The coregulator exchange in transcriptional functions of nuclear receptors. *Genes Dev*. 2000;14(2):121–141.
29. Gwag T, et al. Non-nucleoside reverse transcriptase inhibitor efavirenz activates PXR to induce hypercholesterolemia and hepatic steatosis [published online ahead of print January 21, 2019]. *J Hepatol*. https://doi.org/10.1016/j.jhep.2018.12.038.
30. Kim H, et al. Anti-inflammatory effect of quetiapine on collagen-induced arthritis of mouse. *Eur J Pharmacol*. 2012;678(1-3):55–60.
31. Zhu S, et al. Quetiapine attenuates glial activation and proinflammatory cytokines in APP/PS1 transgenic mice via inhibition of nuclear factor-κB pathway. *Int J Neuropsychopharmacol*. 2014;18:pyu022.
32. He J, et al. Beneficial effects of quetiapine in a transgenic mouse model of Alzheimer's disease. *Neurobiol Aging*. 2009;30(8):1205–1216.
33. Nair AB, Jacob S. A simple practice guide for dose conversion between animals and human. *J Basic Clin Pharm*. 2016;7(2):27–31.
34. Sharma V, McNeill JH. To scale or not to scale: the principles of dose extrapolation. *Br J Pharmacol*. 2009;157(6):907–921.
35. Abumrad NA, Davidson NO. Role of the gut in lipid homeostasis. *Physiol Rev*. 2012;92(3):1061–1085.
36. Hussain MM, Rava P, Walsh M, Rana M, Iqbal J. Multiple functions of microsomal triglyceride transfer protein. *Nutr Metab (Lond)*. 2012;9:14.
37. Dai K, Khatun I, Hussain MM. NR2F1 and IRE1beta suppress microsomal triglyceride transfer protein expression and lipoprotein assembly in undifferentiated intestinal epithelial cells. *Arterioscler Thromb Vasc Biol*. 2010;30(3):568–574.
38. Altmann SW, et al. Niemann-Pick C1 Like 1 protein is critical for intestinal cholesterol absorption. *Science*. 2004;303(5661):1201–1204.
39. Sontag TJ, Chellan B, Getz GS, Reardon CA. Differing rates of cholesterol absorption among inbred mouse strains yield differing levels of HDL-cholesterol. *J Lipid Res*. 2013;54(9):2515–2524.
40. Iqbal J, Parks JS, Hussain MM. Lipid absorption defects in intestine-specific microsomal triglyceride transfer protein and ATP-binding cassette transporter A1-deficient mice. *J Biol Chem*. 2013;288(42):30432–30444.

41. Wang Y, et al. Mice lacking ANGPTL8 (Betatrophin) manifest disrupted triglyceride metabolism without impaired glucose homeostasis. *Proc Natl Acad Sci USA*. 2013;110(40):16109–16114.
42. Quiroga AD, Lian J, Lehner R. Carboxylesterase1/Esterase-x regulates chylomicron production in mice. *PLoS One*. 2012;7(11):e49515.
43. Uchida A, et al. Reduced triglyceride secretion in response to an acute dietary fat challenge in obese compared to lean mice. *Front Physiol*. 2012;3:26.
44. Wang B, et al. Intestinal Phospholipid Remodeling Is Required for Dietary-Lipid Uptake and Survival on a High-Fat Diet. *Cell Metab*. 2016;23(3):492–504.
45. Voshol PJ, et al. Postprandial chylomicron formation and fat absorption in multidrug resistance gene 2 P-glycoprotein-deficient mice. *Gastroenterology*. 2000;118(1):173–182.
46. Zachos NC, et al. Human Enteroids/Colonoids and Intestinal Organoids Functionally Recapitulate Normal Intestinal Physiology and Pathophysiology. *J Biol Chem*. 2016;291(8):3759–3766.
47. Lei NY, et al. Intestinal subepithelial myofibroblasts support the growth of intestinal epithelial stem cells. *PLoS One*. 2014;9(1):e84651.
48. Stoddart CA, et al. Validation of the SCID-hu Thy/Liv mouse model with four classes of licensed antiretrovirals. *PLoS One*. 2007;2(7):e655.
49. Davis HR, et al. Niemann-Pick C1 Like 1 (NPC1L1) is the intestinal phytosterol and cholesterol transporter and a key modulator of whole-body cholesterol homeostasis. *J Biol Chem*. 2004;279(32):33586–33592.
50. Myocardial Infarction Genetics Consortium Investigators, et al. Inactivating mutations in NPC1L1 and protection from coronary heart disease. *N Engl J Med*. 2014;371(22):2072–2082.
51. Bjorn L, Leren TP, Ose L, Hamsten A, Karpe F. A functional polymorphism in the promoter region of the microsomal triglyceride transfer protein (MTP -493G/T) influences lipoprotein phenotype in familial hypercholesterolemia. *Arterioscler Thromb Vasc Biol*. 2000;20(7):1784–1788.
52. Ledmyr H, Karpe F, Lundahl B, McKinnon M, Skoglund-Andersson C, Ehrenborg E. Variants of the microsomal triglyceride transfer protein gene are associated with plasma cholesterol levels and body mass index. *J Lipid Res*. 2002;43(1):51–58.
53. Soh J, Iqbal J, Queiroz J, Fernandez-Hernando C, Hussain MM. MicroRNA-30c reduces hyperlipidemia and atherosclerosis in mice by decreasing lipid synthesis and lipoprotein secretion. *Nat Med*. 2013;19(7):892–900.
54. Iqbal J, Queiroz J, Li Y, Jiang XC, Ron D, Hussain MM. Increased intestinal lipid absorption caused by Ire1β deficiency contributes to hyperlipidemia and atherosclerosis in apolipoprotein E-deficient mice. *Circ Res*. 2012;110(12):1575–1584.
55. Iqbal J, et al. IRE1beta inhibits chylomicron production by selectively degrading MTP mRNA. *Cell Metab*. 2008;7(5):445–455.
56. Sui Y, et al. IKKβ links vascular inflammation to obesity and atherosclerosis. *J Exp Med*. 2014;211(5):869–886.
57. Zhou C, et al. Mutual repression between steroid and xenobiotic receptor and NF-kappaB signaling pathways links xenobiotic metabolism and inflammation. *J Clin Invest*. 2006;116(8):2280–2289.
58. Delfosse V, et al. Synergistic activation of human pregnane X receptor by binary cocktails of pharmaceutical and environmental compounds. *Nat Commun*. 2015;6:8089.
59. Iqbal J, Hussain MM. Evidence for multiple complementary pathways for efficient cholesterol absorption in mice. *J Lipid Res*. 2005;46(7):1491–1501.
60. Wang B, et al. Intestinal Phospholipid Remodeling Is Required for Dietary-Lipid Uptake and Survival on a High-Fat Diet. *Cell Metab*. 2016;23(3):492–504.
61. Jattan J, et al. Using primary murine intestinal enteroids to study dietary TAG absorption, lipoprotein synthesis, and the role of apoC-III in the intestine. *J Lipid Res*. 2017;58(5):853–865.
62. Helsley RN, et al. Targeting IκB kinase β in Adipocyte Lineage Cells for Treatment of Obesity and Metabolic Dysfunctions. *Stem Cells*. 2016;34(7):1883–1895.
63. Sui Y, Park SH, Wang F, Zhou C. Perinatal Bisphenol A Exposure Increases Atherosclerosis in Adult Male PXR-Humanized Mice. *Endocrinology*. 2018;159(4):1595–1608.
64. Wang F, et al. Myeloid β-Catenin Deficiency Exacerbates Atherosclerosis in Low-Density Lipoprotein Receptor-Deficient Mice. *Arterioscler Thromb Vasc Biol*. 2018;38(7):1468–1478.
65. Sui Y, et al. IKKβ is a β-catenin kinase that regulates mesenchymal stem cell differentiation. *JCI Insight*. 2018;3(2):e96660.